Supplementary Information

Ultrathin films of 2D Hofmann-type coordination polymers: influence of pillaring linkers on structural flexibility and vertical charge transport

Víctor Rubio-Giménez,[†] Garin Escorcia-Ariza,[†] Carlos Bartual-Murgui,[†] Christian Sternemann,[‡] Marta Galbiati,[†] Javier Castells-Gil,[†] José Antonio Real,[†] Sergio Tatay[†]* and Carlos Martí-Gastaldo[†]*

[†] Instituto de Ciencia Molecular, Universitat de València, Catedrático José Beltrán 2, 46980 Paterna, Spain
[‡] Fakultät Physik/DELTA, Technische Universität Dortmund, 44221 Dortmund, Germany

Table of contents

Figure SI1. Examples of 3D and 2D Fe^{II}-HCPs. Structures of $[Fe(pz)\{Pt(CN)_4\}]$ (a, pz = pyrazine)[1] and $[Fe(py)_2\{Pt(CN)_4\}]$ (b, py = pyridine).[2] Color code: Fe, red; Pt, turquoise; N, blue; C, gray.

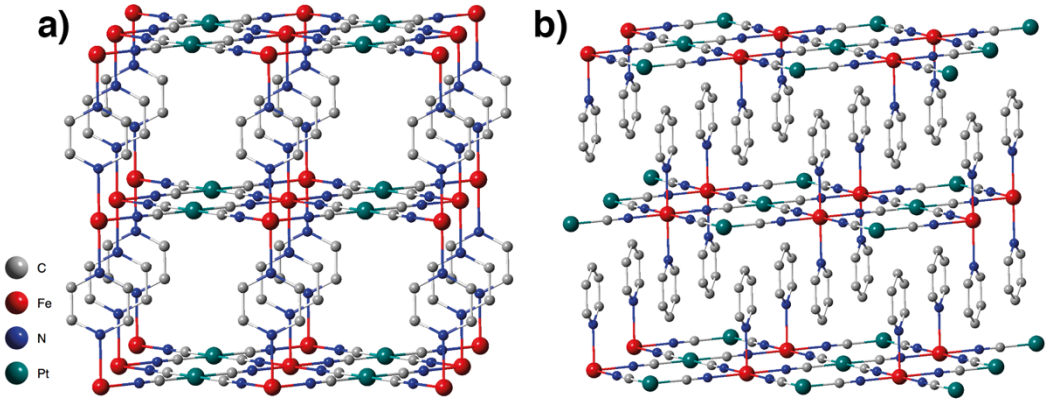

Table SI1. π–π distances between neighboring py, pym and isoq axial ligands in consecutive layers of $[Fe(L)_2\{Pt(CN)_4\}]$ as extracted from single crystal structures (CCDCs 1405911, 1910989 and 1910991).

	Linker		
	py	**pym**	**isoq**
$d_{\pi-\pi}$(Å)	3.779	3.730	3.801*

Table SI2. Atom distances in π–π contacts between neighboring isoq and pym axial ligands in consecutive layers of $[Fe(L)_2\{Pt(CN)_4\}]$ as extracted from as extracted from single crystal structures (CCDCs 1910989 and 1405911).

π-π contact 1 (isoq)*		**π-π contact 2 (isoq)***		**π-π contact (py)**	
Atoms	**d (Å)**	**Atoms**	**d (Å)**	**Atoms**	**d (Å)**
C7-C5	3.76(3)	N1-C9	3.69(3)	N2-C4	3.78(2)
C7-C4	3.72(3)	C1-C9	3.78(3)	C3-C2	3.78(2)
C8-N1	3.77(3)	C2-C4	3.72(3)	C2-C3	3.78(2)
C6-C3	3.68(3)	C3-C4	3.69(3)	C2-C3	3.78(2)
N1-C8	3.77(3)	C3-C3	3.50(2)	C2-C3	3.78(2)
C2-C9	3.73(3)	C9-C5	3.67(3)	C4-N2	3.78(2)
C9-C2	3.73(3)	C9-C1	3.78(3)		
C3-C6	3.68(3)	C4-C2	3.72(3)		
C1-C8	3.64(3)	C5-C9	3.67(3)		
C8-C1	3.64(3)	C8-C5	3.58(2)		
C5-C7	3.76(3)				
C4-C7	3.72(3)				

** For symmetry reasons, the isoq compound shows two crystallographycally different π-π contacts. Hence, the π-π centroid-centroid distance for $[Fe(isoq)_2\{Pt(CN)_4\}]$ is an average of two distances.*

Figure SI2. LeBail refinements of bulk $[Fe(L)_2\{Pt(CN)_4\}]$ [L = py (a), pym (b) and isoq (c)] samples.

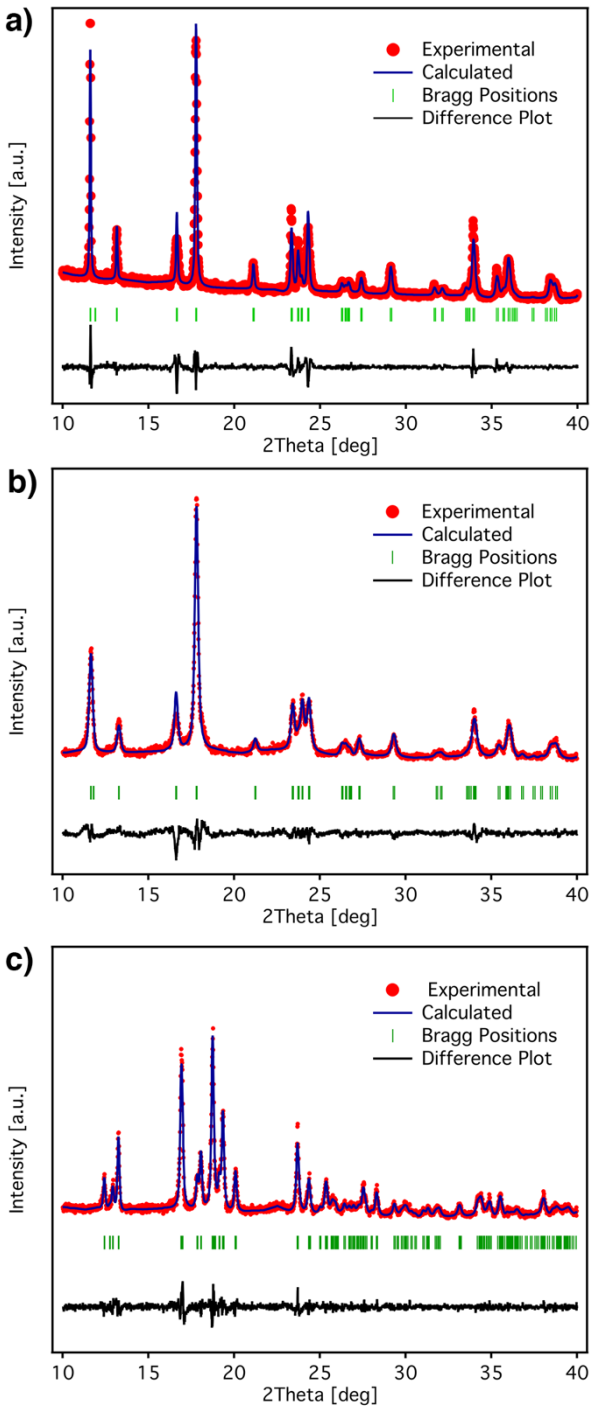

Table SI3. Summary of the parameters obtained from the LeBail refinements of Figure SI2.

L	Space group	a [Å]	b [Å]	c [Å]	V [Å^3]	R_p [%]	R_{wp} [%]	R_{exp} [%]	GoF
py	Orthorhombic, Cmmm	7.5009	15.2463	7.4374	850	7.5	10.1	6.5	1.5
pym	Orthorhombic, Cmmm	7.4215	15.1962	7.4938	845	8.5	11.0	8.0	1.4
isoq	Triclinic, P-1	7.3019	7.5184	10.4595	519	12.5	16.4	11.7	1.4

Table SI4. Elemental analysis results for bulk $[Fe(L)_2\{Pt(CN)_4\}]$ [L = py, pym and isoq] samples.

L	Calculated			Found		
	C (%)	H (%)	N (%)	C (%)	H (%)	N (%)
py	32.77	1.96	16.36	33.20	2.14	16.10
pym	27.03	1.89	21.02	27.13	1.77	20.42
isoq	43.08	2.30	13.70	42.79	2.24	13.20

Figure SI3. IRRAS spectra of Si/Ti (3 nm)/Au (150 nm)/[Fe(L)$_2${Pt(CN)$_4$}] [L = py (a), pym (b) and isoq (c)] film samples (in green) compared with the FT-IR spectra of their respective bulk analogues (in red). Assigned vibrations are highlighted in gray. Abbreviations: ν, stretching; δ, in-plane bending; br, breathing; γ, out-of-plane bending. Assigned vibrations are highlighted in gray.

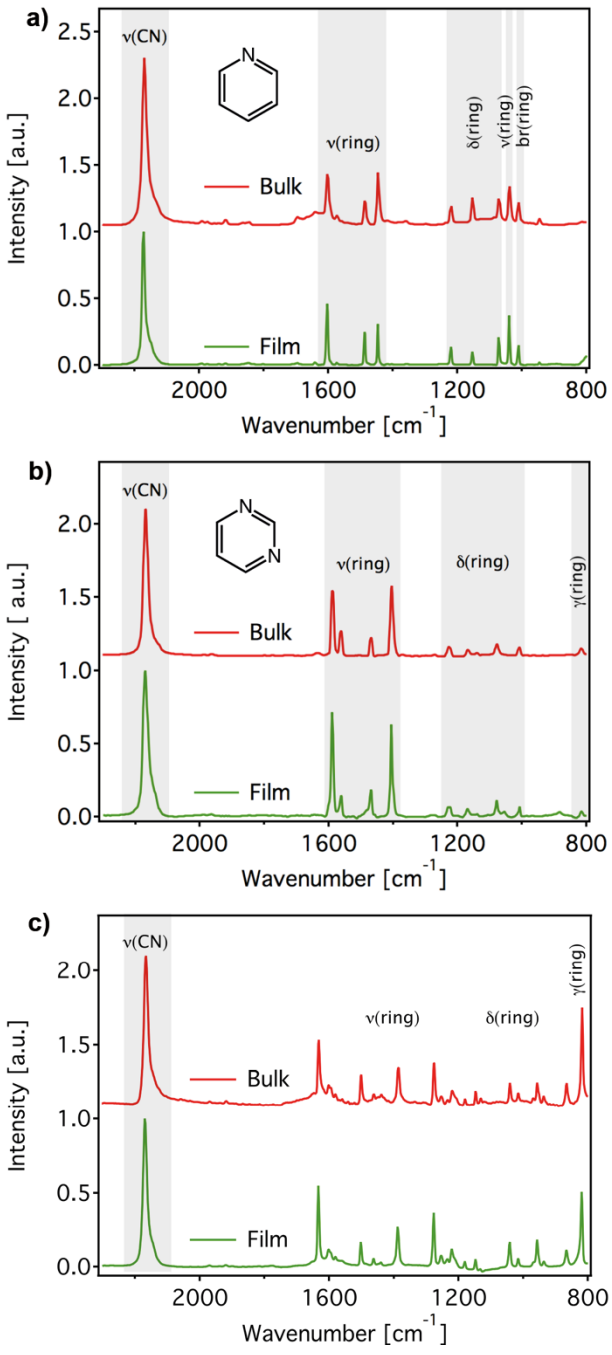

Figure SI4. Survey XPS spectra of a 30-cycles Si/Ti (3 nm)/Au (15 nm)/[$Fe(L)_2\{Pt(CN)_4\}$] film samples (in green) compared with their respective bulk analogues (in red). Assigned peaks are highlighted in gray.

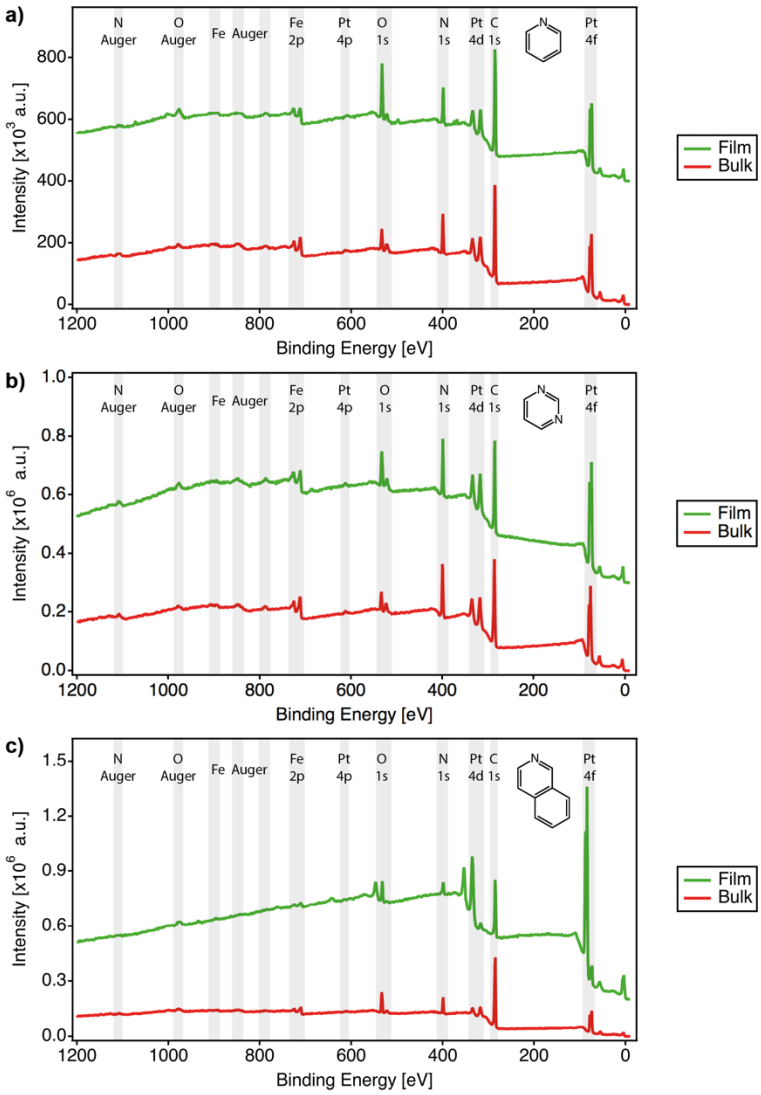

Table SI5. XPS data for Si/Ti (3 nm)/Au (15 nm)/[$Fe(L)_2\{Pt(CN)_4\}$] (L = py, pym and isoq) films and respective bulk samples extracted from high-resolution spectra. Units are eV in all cases.

L = py	**Fe 2p**			**Pt 4f**		
Number of cycles	**BE $2p_{3/2}$**	**BE $2p_{1/2}$**	**ΔE**	**BE $4f_{7/2}$**	**BE $4f_{5/2}$**	**ΔE**
Bulk	710.1	723.8	13.7	73.8	77.1	3.3
30	710.3	724.0	13.7	73.8	77.1	3.3
20	710.0	723.7	13.7	74.0	77.3	3.3
10	710.1	724.0	13.9	74.1	77.4	3.3
5	710.0	723.8	13.8	74.0	77.2	3.2
3	710.3	724.1	13.8	74.1	77.2	3.1

L = pym	**Fe 2p**			**Pt 4f**		
Number of cycles	**BE $2p_{3/2}$**	**BE $2p_{1/2}$**	**ΔE**	**BE $4f_{7/2}$**	**BE $4f_{5/2}$**	**ΔE**
Bulk	710.7	724.3	13.6	73.5	76.9	3.4
30	710.9	724.4	13.5	73.6	76.9	3.3
20	711.2	724.9	13.7	73.7	77.0	3.3
10	710.7	724.5	13.8	73.6	76.9	3.3
5	710.7	724.5	13.8	73.6	76.9	3.3
3	710.3	724.1	13.8	73.5	77.0	3.5

L = isoq	**Fe 2p**			**Pt 4f**		
Number of cycles	**BE $2p_{3/2}$**	**BE $2p_{1/2}$**	**ΔE**	**BE $4f_{7/2}$**	**BE $4f_{5/2}$**	**ΔE**
Bulk	709.1	723	13.9	73.5	76.8	3.3
30	709.4	723.3	13.9	73.7	77.0	3.3
20	709.9	723.6	13.7	73.6	76.9	3.3
10	709.8	723.5	13.7	73.7	77.0	3.3
5	709.9	723.7	13.8	73.6	76.9	3.3
3	710.6	723.5	12.9	73.5	76.7	3.2

Figure SI5. High-resolution XPS spectra of the N 1s and C 1s regions for a set of films and bulk samples for L = py (a), pym (b) and isoq (c). (Below) N/Fe (d) and C/Fe (e) ratios for the same samples calculated by peak integration along with theoretical ratios calculated with the respective chemical formulas (dashed gray lines). We attribute the disparity in C/Fe ratios to the presence of adventitious carbon species on the surface of the samples.

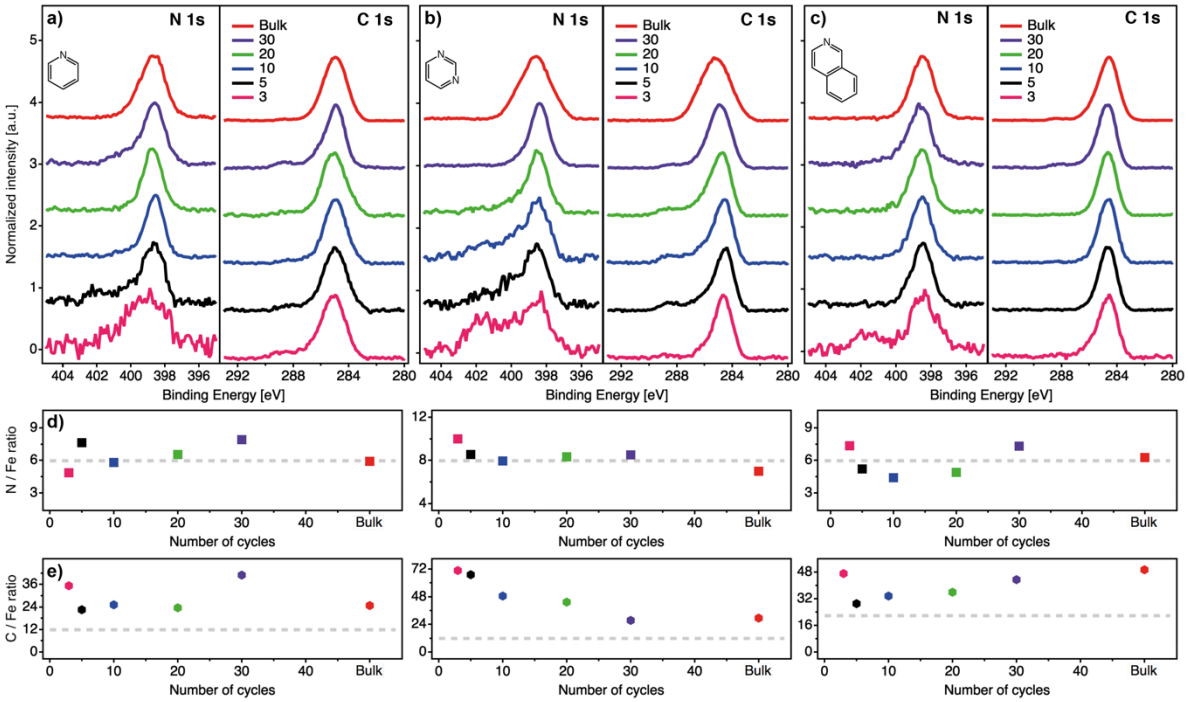

Figure SI6. 2D-GIXRD images for a set of 30-cycle $[Fe(L)_2\{Pt(CN)_4\}]$ films of L = py (a), pym (b) and isoq (c).

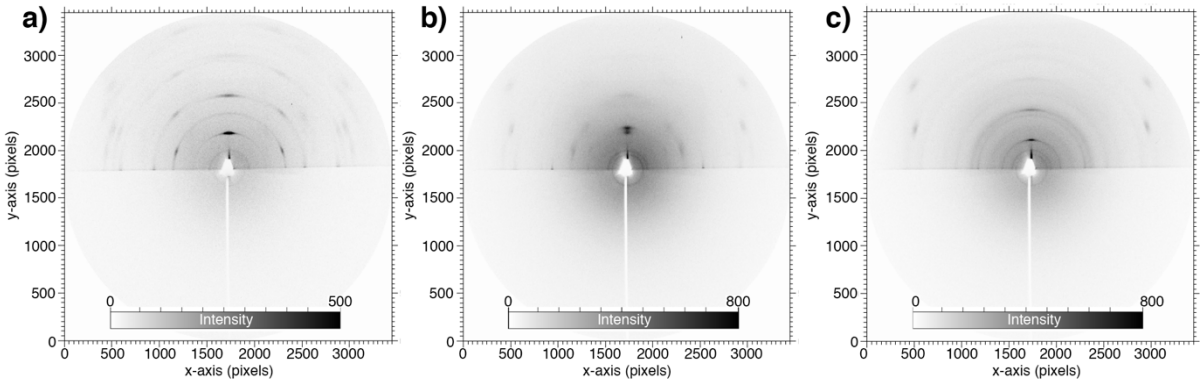

Figure SI7. Diffractograms of the complete integration of GIXRD patterns a set of 30-cycle $[Fe(L)_2\{Pt(CN)_4\}]$ films of L = py (a), pym (b) and isoq (c), along with their respective bulk PXRD and simulated (without preferred orientation) diffractograms.

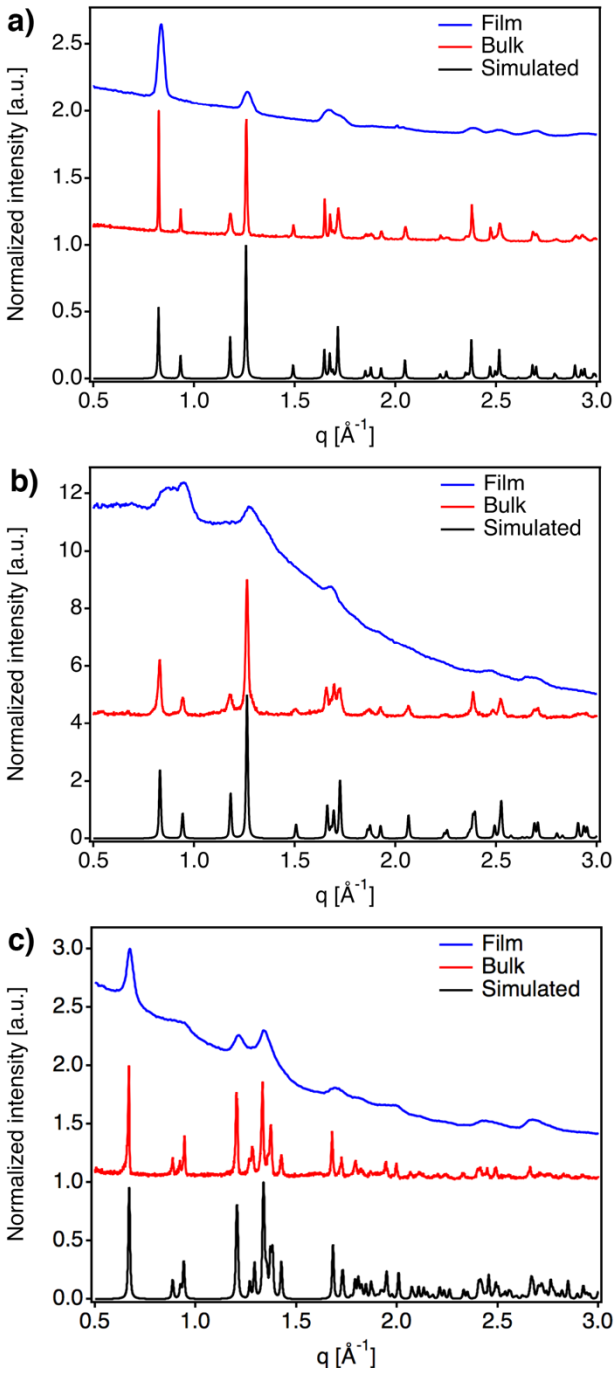

Figure SI8. Additional 1 x 1 μm^2 AFM topography images for Si/Ti (3 nm)/Au (15 nm)/[Fe(L)$_2${Pt(CN)$_4$}] 3, 7 and 15 cycles films of py (a, b, c), pym (d, e, f) and isoq (g, h, i).

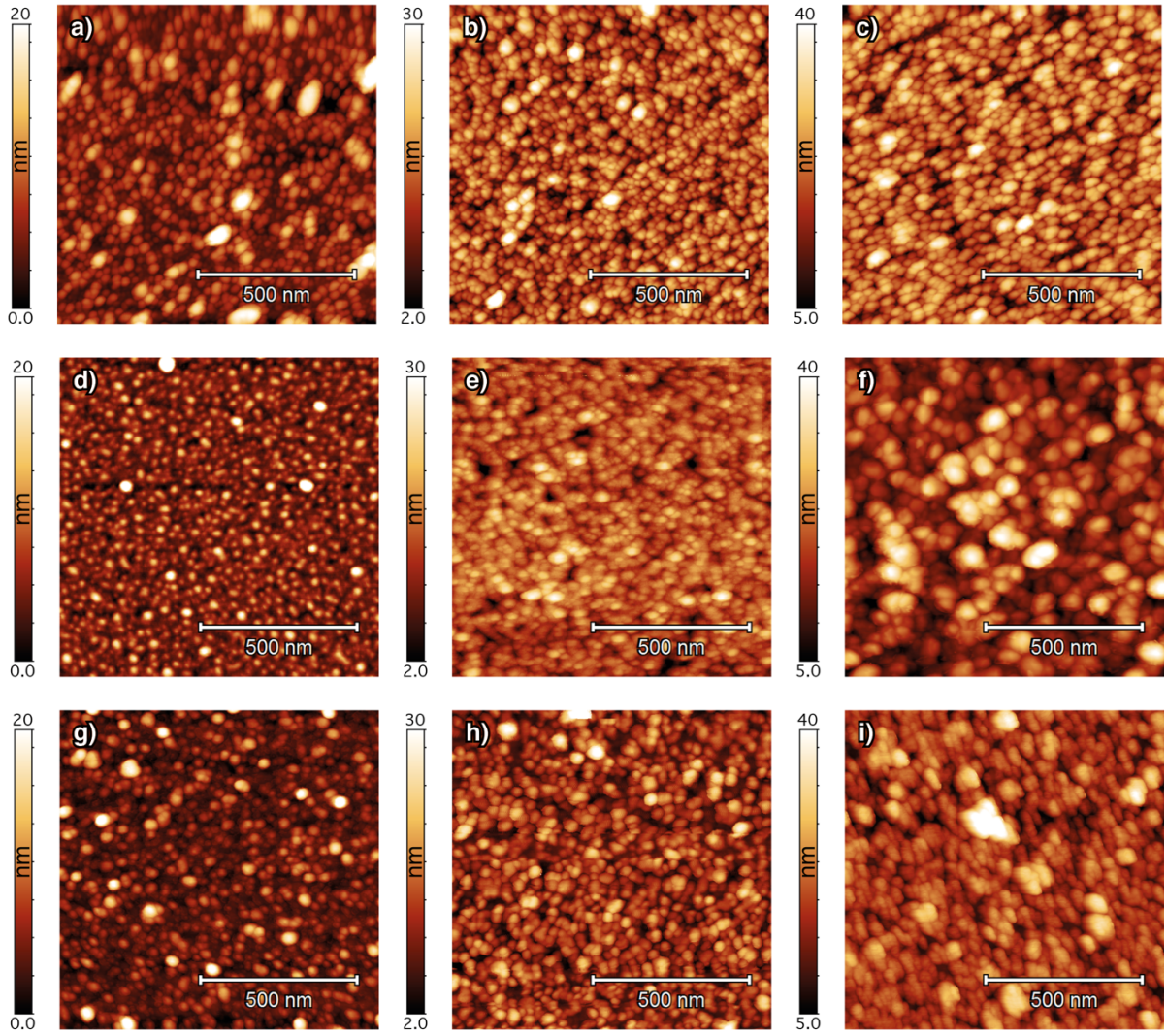

Figure SI9. (a-c) Evolution of RMS roughness values for Si/Ti (3 nm)/Au (15 nm)/[Fe(L)$_2${Pt(CN)$_4$}] films with the number of cycles, which shows an exponential-like increase from ~1 nm for 1 cycle to ~5.5 nm after 10-15 cycles. Values were calculated by analyzing 1 x 1 μm^2 AFM topography images with the Gwyddion software package.[3]

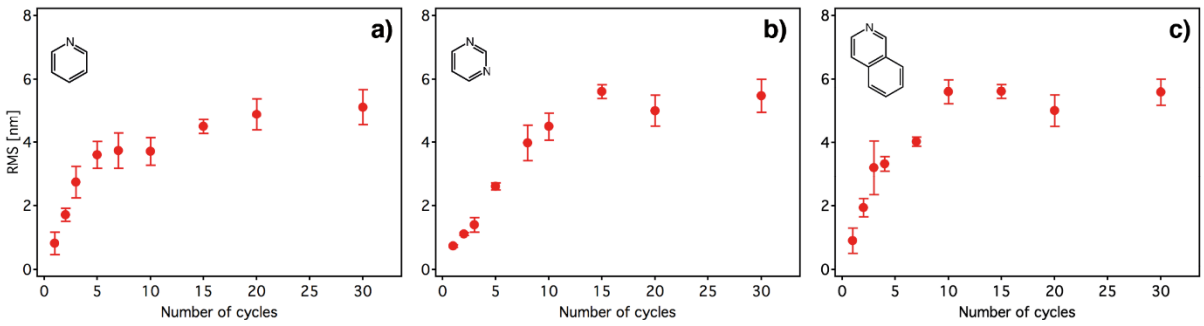

Figure SI10. Methanol sorption of bulk [Fe(isoq)$_2${Pt(CN)$_4$}]. a) Methanol adsorption/desorption isotherms at 298 K of bulk [Fe(isoq)$_2${Pt(CN)$_4$}]. b) PXRD patterns of bulk [Fe(isoq)$_2${Pt(CN)$_4$}] powder samples as-synthesized and after a methanol adsorption/desorption cycle. c) LeBail refinements of a bulk [Fe(isoq)$_2${Pt(CN)$_4$}] powder sample after a methanol adsorption/desorption cycle. Refined Cell Parameters: Triclinic, *P-1*, a = 7.3029 Å, b = 7.4895 Å, c = 10.4433 Å, α = 107.81º, β = 107.58º, γ = 89.95º, V = 516 Å^3, R_p = 2.15 %, R_{wp} = 2.80 %, R_{exp} = 2.62 % GoF = 1.1.

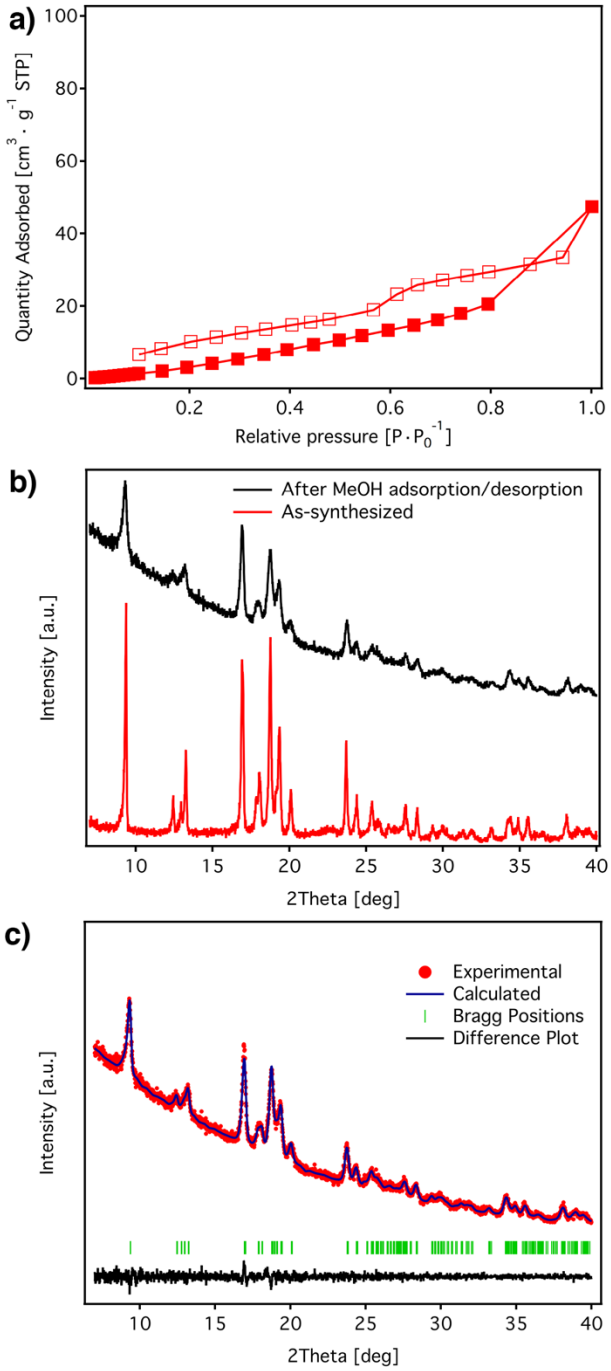

Figure SI11. Scheme of the experimental set-up for the in situ XRD measurements of $[Fe(isoq)_2\{Pt(CN)_4\}]$ thin films under volatile solvents. This features two He currents, the dilution gas (top) and the carrier gas (bottom). The latter flows through a bubbler that contains the volatile solvent, yielding a solvent-saturated He mixture, which will later mix with the carrier gas and then pass through the sample in the doomed stage.

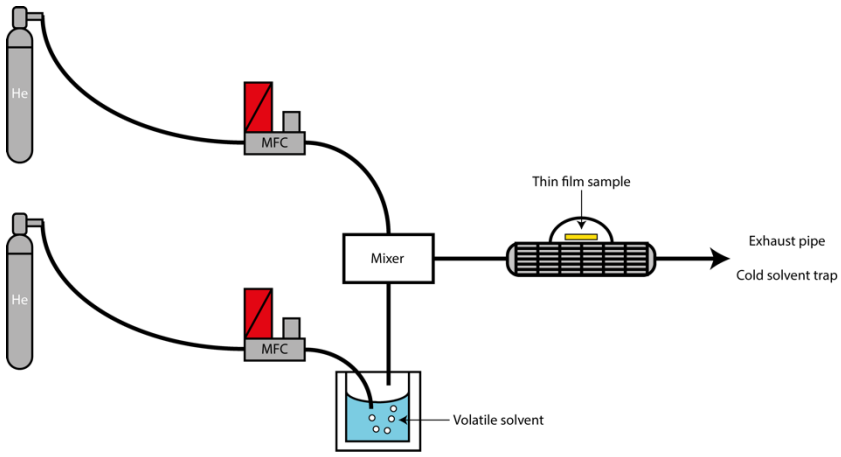

Figure SI12. LeBail refinements of a the full out-of-plane XRD patterns of $[Fe(isoq)_2\{Pt(CN)_4\}]$ ultrathin film (30-cycles) under different He-solvent mixtures.

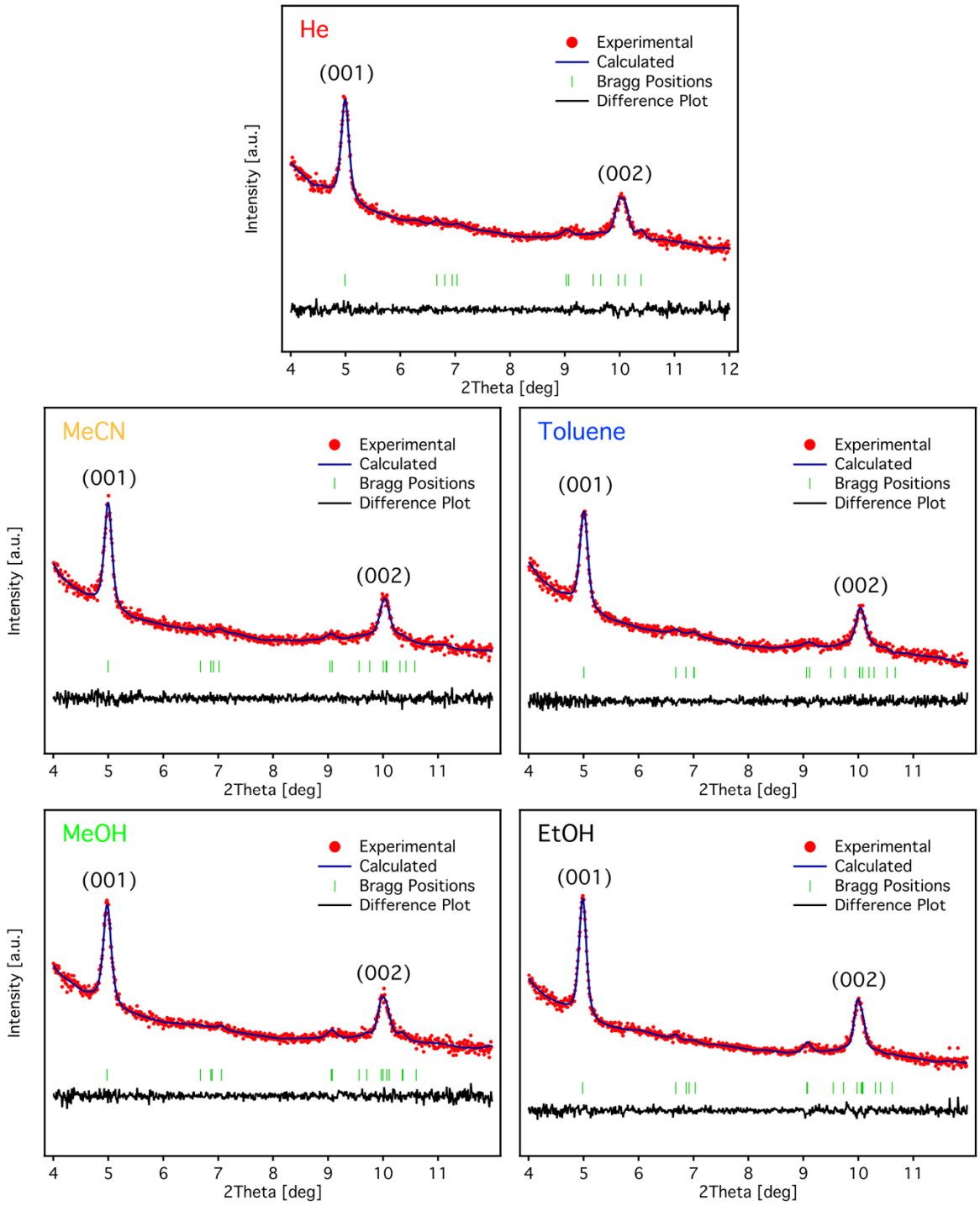

Table SI6. Summary of the parameters obtained from the LeBail refinements of Figure SI12.

Solvent	Space group	c [Å]	R_p [%]	R_{wp} [%]	R_{exp} [%]	GoF
He	Triclinic, P-1	10.49523	1.9	2.3	1.5	1.5
MeCN	Triclinic, P-1	10.58511	2.0	2.5	2.0	1.3
Toluene	Triclinic, P-1	10.50537	2.0	2.5	1.8	1.4
MeOH	Triclinic, P-1	10.59822	1.9	2.4	1.6	1.5
EtOH	Triclinic, P-1	10.57973	1.9	2.3	1.5	1.6

Figure SI13. View along the a axis of $[Fe(py)_2\{Pt(CN)_4\}]$ (a), $[Fe(pym)_2\{Pt(CN)_4\}]$ (b) and $[Fe(isoq)_2\{Pt(CN)_4\}]$ (c) structures together with simulated Connolly surface areas (in yellow) for a Connolly radius of 1.2 Å. Surface area simulations were carried out using molecular simulation software Materials Studio 2017 R2 (Accelrys Inc.).

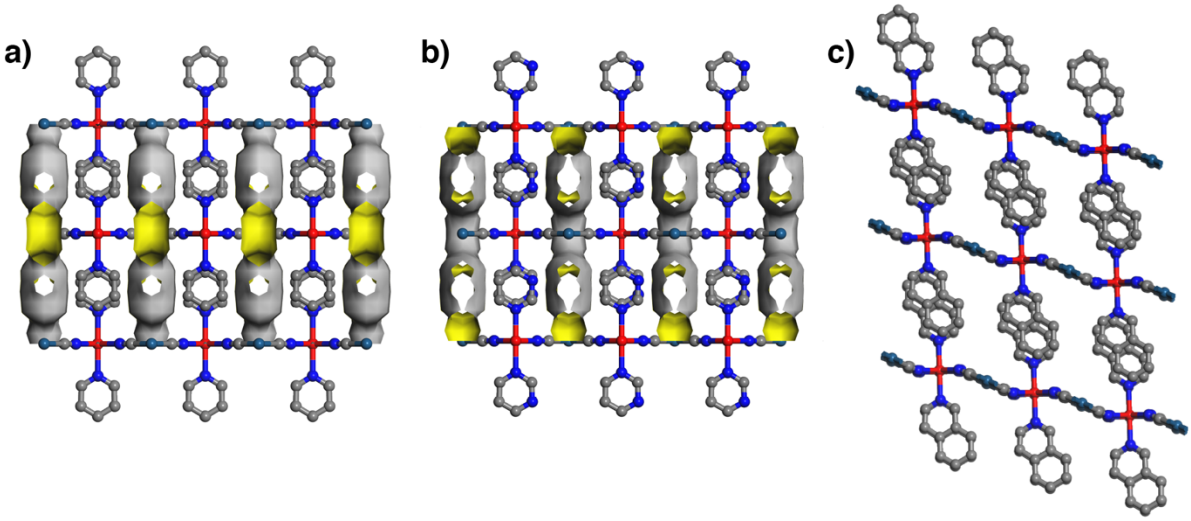

SI1. Electrical characterization of 2D Fe^{II}-HCP films.

We measured the current (I) as function of the applied bias (V) of the junctions formed by bringing a gallium-indium eutectic (EGaIn) liquid-metal drop into contact with the surface of 2D Fe^{II}-HCPs using the gold film as bottom electrode. The area of the contact was estimated from the diameter of the contact zone, which was measured using a CCD camera. Data was recorded using a Keithley 6517B electrometer controlled with LabVIEW (National Instruments). EGaIn drops with drop radius 75 µm were reproducibly produced using a Hamilton syringe. A scheme of the experimental set-up used is shown on Figure SI14.

Figure SI14. Scheme of the set-up used for 2D Fe^{II}-HCP electrical characterization.

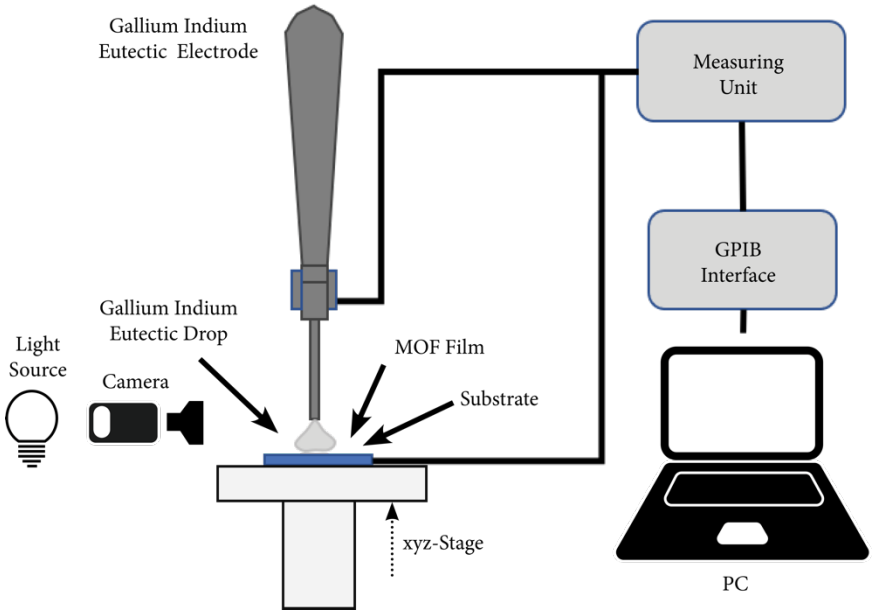

We measured three consecutive I-V curves for a given drop size. From these data, we calculated the current density ($J = I/A$) versus voltage applied as shown in Figure SI15.

Figure SI15. Logarithm of the current density as function of the bias voltage calculated from three consecutive I-V curves measures on a $[Fe(isoq)_2\{Pt(CN)_4\}]$ 5-cycles film.

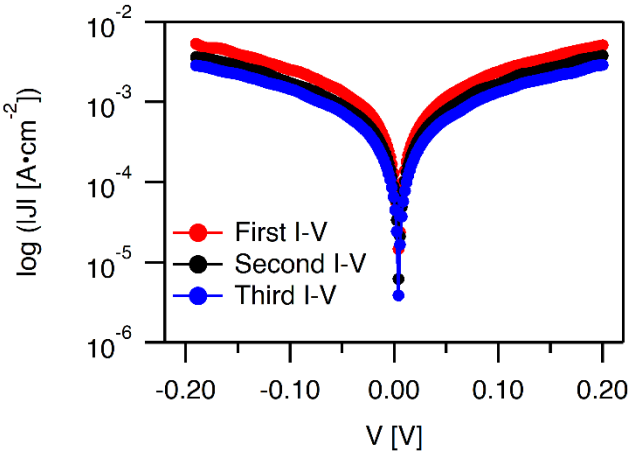

For each series of contacts, we calculated the current density at ± 0.12 V. The value of J obtained at a certain V is expected to be roughly constant.

Once the three I-V curves are recollected, we displaced the sample laterally with an xyz-stage, produced a new EGaIn drop and repeated the process all over again. To improve statistic, we repeated this process at least 10 times on different parts of the film's surface and collected at least 30 curves I-V curves for each sample Figure SI16a. The experimental variation in the J-V curves collected for a given sample can be attributed to the presence of small local variation on thickness, roughness or structure and/or to errors on the estimation of the drop diameter. As displayed in Figure SI16b this variation leads to roughly normally distributed J values for each sample. The center of this distribution corresponds to the average J of the sample.

Figure SI16. a) All 30 J-V curves measured for a 5-cycles 2D Fe^{II}-HCP film. b) Logarithm of J histogram at ± 0.12 V extracted from the J-V curves displayed in a). Bolder lines correspond to the average and Gaussian fit to the data, respectively.

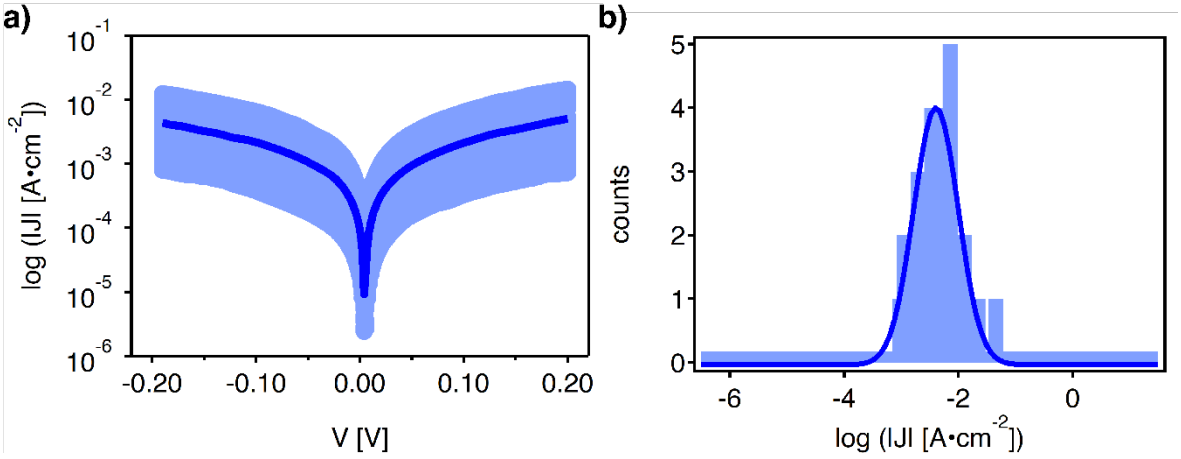

Figure SI17. [Fe(L)$_2${Pt(CN)$_4$}] (L = py, pym and isoq) average log J-V curves as a function of the number of cycles. Curves are the average of at least 30 J-V curves measured at various positions over the surface of each film.

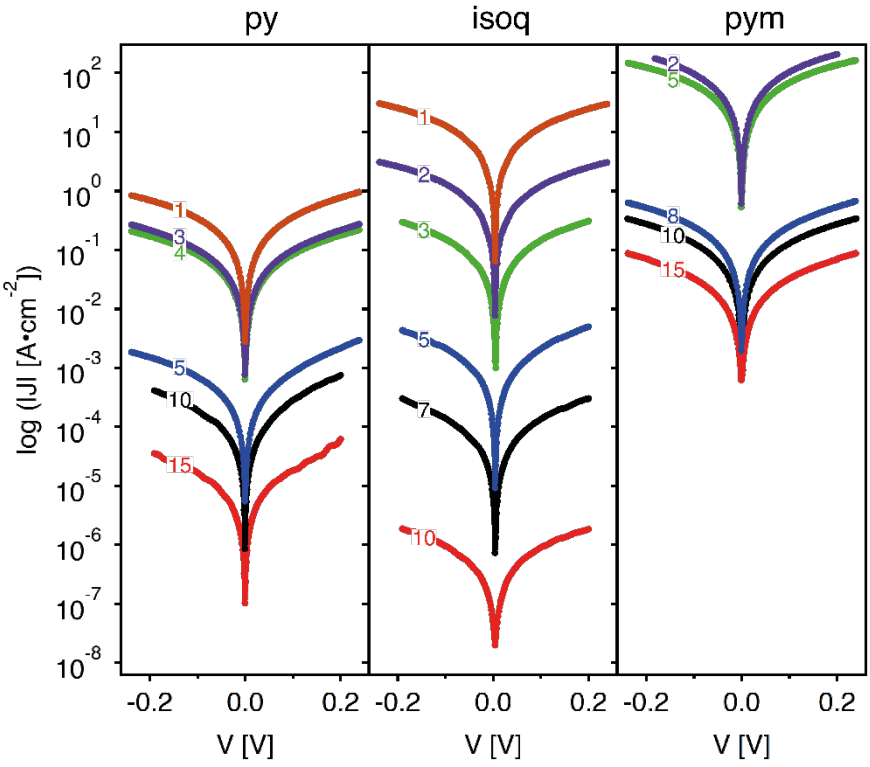

References

[1] Niel, V., Martinez-Agudo, J. M., Muñoz, M. C., Gaspar, A. B., Real, J. A., *Inorg. Chem.* **2001**, *40*, 3838-3839.
[2] Sakaida, S., Otsubo, K., Sakata, O., Song, C., Fujiwara, A., Takata, M., Kitagawa, H., *Nat. Chem.* **2016**, *8*, 377-383.
[3] Nečas, D., Klapetek, P., *Cent. Eur. J. Phys.* **2012,** *10*, 181-188.